

This work was written as part of one of the author's official duties as an Employee of the United States Government and is therefore a work of the United States Government. In accordance with 17 U.S.C. 105, no copyright protection is available for such works under U.S. Law.

Public Domain Mark 1.0

<https://creativecommons.org/publicdomain/mark/1.0/>

Access to this work was provided by the University of Maryland, Baltimore County (UMBC) ScholarWorks@UMBC digital repository on the Maryland Shared Open Access (MD-SOAR) platform.

**Please provide feedback**

Please support the ScholarWorks@UMBC repository by emailing [scholarworks-group@umbc.edu](mailto:scholarworks-group@umbc.edu) and telling us what having access to this work means to you and why it's important to you. Thank you.

# Aerosol detection by TOMS and POLDER over oceanic regions

Isabelle Chiapello, Philippe Goloub, Didier Tanré, and Aurelia Marchand

Laboratoire d'Optique Atmosphérique, Université des Sciences et Technologies de Lille, Villeneuve d'Ascq, France

Jay Herman, and Omar Torres

Laboratory for Atmospheres, NASA Goddard Space Flight Center, Greenbelt, Maryland

**Abstract.** In this paper we investigate the aerosol content retrieved by Earth-Probe Total Ozone Mapping Spectrometer (TOMS) and ADEOS POLDER over oceanic regions for the period November 1996 to June 1997. We combine the aerosol index (AI) derived from TOMS corresponding to UV-absorbing aerosols (desert dust and biomass-burning particles) and the POLDER aerosol optical thickness (AOT) and Angström coefficients. The seasonal composited images from the two sensors show in general consistent spatial distributions of the aerosol over oceans, with the highest aerosol content retrieved over the north tropical and equatorial Atlantic. Over the different oceanic regions investigated (i.e., Atlantic Ocean, Mediterranean Sea, Indian Ocean, and Pacific Ocean), TOMS and POLDER show a good correspondence in the aerosol seasonal variability. At all sites with the exception of the region of the Sea of Japan, we show that during the time periods of maximum aerosol amounts, a linear correlation exists between the TOMS AI and POLDER AOT. For the Sea of Japan the influence of different aerosol types (i.e., desert dust and sulfates) is likely to complicate the TOMS detection. For the other oceanic regions, our results suggest a large variability in the relationship between the TOMS AI and the POLDER AOT, which is likely to be related to changes in aerosol composition and/or altitude.

## 1. Introduction

Despite its inherent difficulties, remote sensing of tropospheric aerosol from space remains a powerful method to provide good spatial coverage, or in some cases a global view of the atmospheric aerosol system. In recent years, several studies have investigated the retrieval of aerosol spatial distribution and variation with time using sensors such as Meteosat [Jankowiak and Tanré, 1992; Moulin *et al.*, 1997a, 1997b; Moulin *et al.*, 1998], Advanced Very High Resolution Radiometer (AVHRR) [Swap *et al.*, 1996; Husar *et al.*, 1997], and Total Ozone Mapping Spectrometer (TOMS) [Herman *et al.*, 1997; Torres *et al.*, 1998]. The derived information is of first importance to improve the current knowledge of the aerosol system and its effect on climate [Kaufman *et al.*, 1997].

Recently, different original approaches have been developed in order to progress in the field of aerosol monitoring from space. The total ozone mapping spectrometer (TOMS) and polarization and directionality of the Earth's reflectances (POLDER) instruments provide new capabilities for deriving aerosol distributions. TOMS allows the real-time retrieval of the distribution of aerosols in the ultraviolet over both continents and oceans by means of a parameter known as aerosol index (AI), which is generally greater than zero for absorbing aerosols (desert dust, carbonaceous aerosols, and volcanic ash) and less than zero for non-absorbing aerosols (sulfate particles) [Herman *et al.*, 1997; Torres *et al.*, 1998].

From the spectral information contained in AI, aerosol optical depth and single-scattering albedo can be derived [Torres *et al.*, 1998]. POLDER, through multispectral, multiangular, and polarization measurements, improves the estimation of aerosol optical thickness (AOT) and provides additional information on aerosol properties through the Angström coefficient [Goloub *et al.*, 1999; Deuzé *et al.*, 1999].

In this context, it seems important to examine the consistency of the aerosol retrieval from these different approaches. By combining the aerosol observations from different sensors, one should be able to better understand the nature of the information retrieved by each instrument. In the regions where the aerosol load is dominated by UV-absorbing particles (i.e., desert dust and biomass burning) we expect good agreement between the geographical distribution of the aerosol as retrieved by the two sensors and good correlation between the aerosol content retrieved by POLDER and the positive values of the TOMS AI. A more detailed quantitative comparison of TOMS and POLDER optical depths is currently underway and will be published separately.

## 2. TOMS and POLDER Aerosol Products

Both POLDER and TOMS instruments were aboard the Japanese ADEOS platform (Advanced Earth Observing System) launched in August 1996 and which made measurements until June 29, 1997. Moreover, the TOMS instrument aboard the Earth-Probe platform made measurements at the same time as ADEOS and continues to provide data today.

The POLDER algorithm for the derivation of the aerosol properties is detailed by Goloub *et al.* [1999] and Deuzé *et al.* [1999]. It should be noted that in the present algorithm the

Copyright 2000 by the American Geophysical Union.

Paper number 1999JD901048.  
0148-0227/00/1999JD901048\$09.00

aerosols are considered nonabsorbing, which means that the aerosol optical thickness (AOT) retrieved by POLDER should be considered as a scattering aerosol optical thickness. The POLDER ADEOS aerosol products have been validated against ground-based Sun photometer measurements from the Aerosol Robotic Network (AERONET) [Holben *et al.*, 1998]. The validation of the POLDER derived AOT at 865 nm over the ocean has shown that the POLDER retrieval is excellent for optical thickness up to 0.8. This agreement also suggests a limited contribution of the absorption to the global AOT. The Angström coefficient is well correlated with the AERONET data, although underestimated (30%) [Goloub *et al.*, 1999]. It should be noted that due to the threshold used in the cloud detection scheme, only aerosol events with AOT lower than 1 (at 865 nm) can be detected by POLDER, which may lead to some systematic underestimation of the mean aerosol content [Deuzé *et al.*, 1999].

A detailed description of the TOMS aerosol index (AI) product is given by Herman *et al.* [1997] and Torres *et al.* [1998]. Briefly, the AI is a measure of the wavelength dependent change of Rayleigh scattered radiance resulting from the competing effects of aerosol scattering and absorption relative to a pure Rayleigh atmosphere [Hsu *et al.*, 1999]. For the Earth-Probe TOMS and ADEOS TOMS instruments, the AI is calculated using the ratio of the radiance between the 331- and 360-nm channels. The AI is defined so that positive values generally correspond to UV-absorbing aerosols and negative values to nonabsorbing aerosols. Since the UV surface reflectivity is low over both land and water [Herman and Celarier, 1997], this method allows the detection of aerosols over both kind of surfaces. Because the Earth-Probe TOMS AI measurements have been found to be closely correlated to ground-based measurements of optical depth [Hsu *et al.*, 1999], we choose to use data from Earth-Probe TOMS rather than ADEOS TOMS in this study, even though the difference in equator crossing time between the Earth-Probe and ADEOS spacecrafts is about 35 min. Another advantage of using Earth-Probe TOMS data is that the "footprint" size of the measurement is smaller compared to ADEOS TOMS (24 x 24 km<sup>2</sup> instead 40 x 40 km<sup>2</sup> at nadir). As a consequence, the daily data from Earth-Probe TOMS have better spatial resolution than other TOMS instruments but have gaps between orbits corresponding to 40% of the Earth's surface.

Correlative analysis of the TOMS-derived AI have been performed using both Sun photometer AOT measurements from the AERONET network and measurements of mineral dust concentrations from different aerosol monitoring stations of the North Atlantic Ocean [Hsu *et al.*, 1999; Chiapello *et al.*, 1999]. These comparisons have demonstrated that there is a linear relationship between the AI derived from TOMS and the Sun photometer AOT over regions of biomass burning and African dust, even though the TOMS detection is dependent on the altitude of the aerosol layer and the nature of the aerosol, as predicted by theoretical simulations [Torres *et al.*, 1998].

For this study our comparison between the TOMS and POLDER aerosol products will be limited to the 8-month lifetime of POLDER ADEOS (November 1996 to June 1997). However, it should be noted that additional flights of POLDER instruments are planned over the next decade. Since the POLDER aerosol products have not been validated over

land surfaces, we will limit our comparisons with TOMS to oceanic regions. Finally, we will consider only the positive values of the TOMS AI, so that the TOMS data will show mainly the UV-absorbing aerosols, that is, desert dust and carbonaceous aerosols. In some instances this will produce an apparent discrepancy between the TOMS data (with sulfates purposely omitted) and the POLDER retrieval that includes both types.

The POLDER aerosol products are delivered over a grid of 18 x 18 km<sup>2</sup>, whereas the TOMS data used in this study are uniformly gridded level-3 product (1°latitude x 1.25°longitude, approximately 110 x 138 km<sup>2</sup> at low latitudes).

### 3. Global Aerosol Distributions Over Oceans

Plate 1 shows the global distributions of the absorbing AI derived from Earth-Probe TOMS (over both continents and oceans) and of AOT at 865 nm and Angström coefficient (865-670 nm) derived from ADEOS POLDER (over oceans only). The results are presented in four maps of 2-month averaged products, for the 8-month time period of data available for this study (from November 1996 to June 1997). Both POLDER and TOMS images show that over oceanic regions most of the aerosol content is located over the north tropical Atlantic, west of the African coast. Accordingly with observations from other sensors such as AVHRR [Husar *et al.*, 1997], the north tropical Atlantic appears to be the oceanic region where the largest and more persistent aerosol amounts are found. POLDER and TOMS show very consistent seasonal shifts of the aerosol plume in this region. The plume is at its maximum extent in May-June, when it reaches into the Caribbean. During the winter (January-February) the plume is located further south due to the seasonal shift of the Intertropical Convergence Zone. In general, the POLDER Angström coefficients show values lower than 0.6 in the north tropical Atlantic region, as expected under the influence of coarse mode particles of Saharan dust. Over the equatorial Atlantic, west of the Gulf of Guinea, the most intense plume appears in January-February and is probably associated with both dust and biomass burning aerosols. Indeed, it has been shown in this region that winter is the season when mineral dust from Sahara and Sahel is transported over the Gulf of Guinea in the low latitudes and toward South America [Morales, 1979; Prospero *et al.*, 1981]. It is remarkable to note that over both equatorial and north tropical Atlantic the aerosol plumes retrieved by POLDER and TOMS have very similar dimensions and show the same seasonal variabilities as that observed by AVHRR [Swap *et al.*, 1996; Husar *et al.*, 1997].

Both TOMS and POLDER show a biomass burning signal over the south tropical Atlantic, west of the coast of Angola. The plume appears in May-June, which corresponds to the beginning of the season of the southern Africa savanna and grassland fires, which occur mostly in July-September [Andreae *et al.*, 1994]. The high Angström coefficients retrieved by POLDER in this region are consistent with submicronic fire smoke particles. For the other oceanic regions, both POLDER and TOMS show much more moderate aerosol amounts than over the Atlantic Ocean, with POLDER AOT below 0.4 and TOMS AI below 1. In general, POLDER seems to detect more aerosols than TOMS does, especially

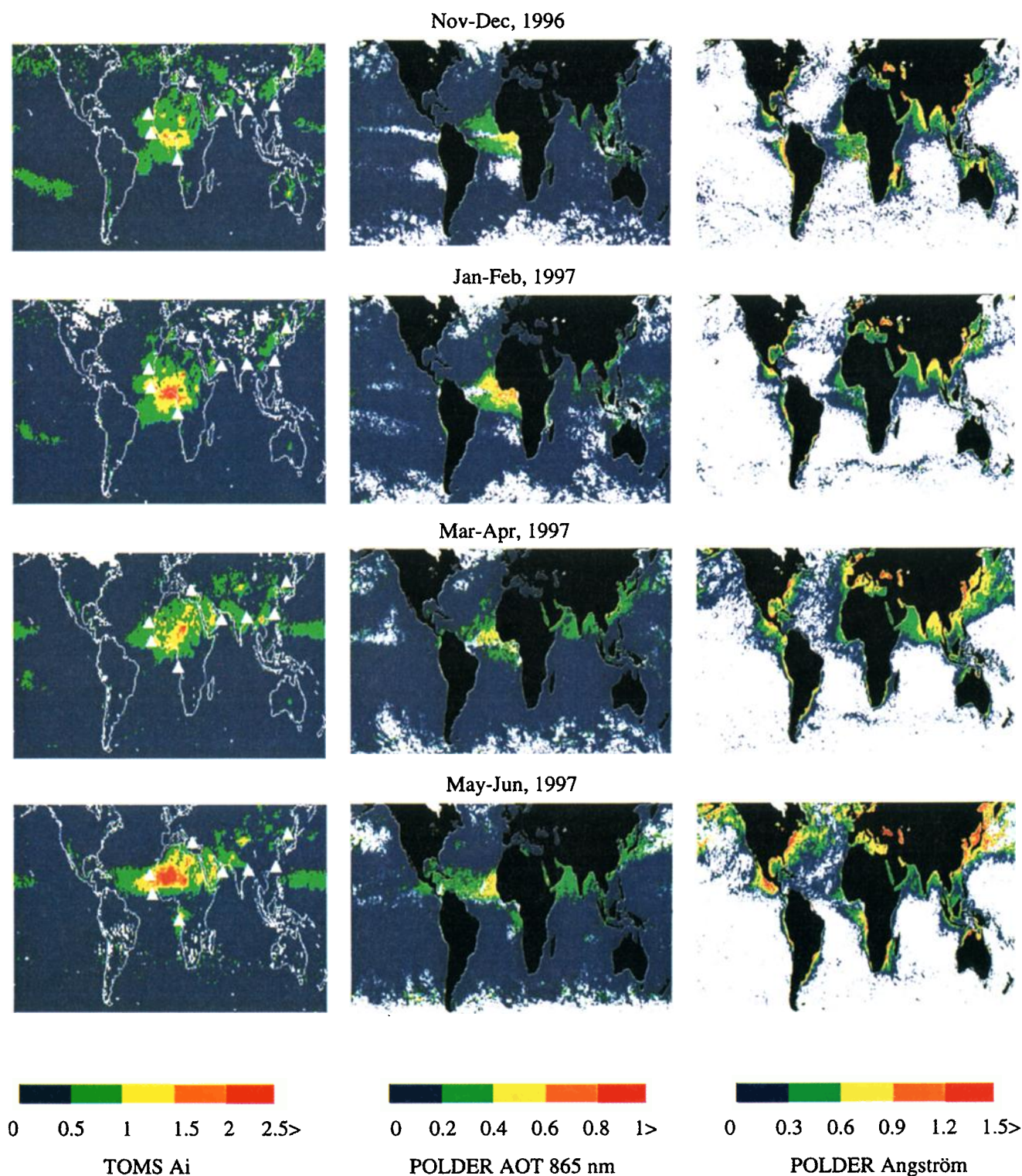


**Plate 1.** Global distributions of Earth-Probe TOMS-derived absorbing aerosol index, ADEOS POLDER-derived aerosol optical thickness at 865 nm, and Angström coefficient (865-670 nm) for the four 2-month time periods between November 1996 and June 1997. Note that when the POLDER-retrieved aerosol optical thickness is less than 0.1, no retrieval is made for the Angström exponent. These areas corresponding to "no retrieval" are in white on Plate 1. The TOMS aerosol index is retrieved over both oceanic and continental surfaces, whereas the POLDER products are shown over oceanic regions only. The white triangles indicate the regions for which the retrieval of aerosol by TOMS and POLDER are compared.



over the Indian Ocean (off the coast of Arabia and India) and over the Pacific Ocean (off the coast of Asia). These differences may be explained by the presence of non-UV-absorbing aerosols (sulfates particles, not included in the positive AI values) or the lower altitude of the aerosol layer which makes the TOMS retrieval of AI less sensitive to absorbing aerosols. Moreover, the transport of mineral dust particles over the Arabian Sea is known to occur mainly in summer (from July to August) [Husar *et al.*, 1997]. This can explain the rather moderate signal detected by TOMS and POLDER over this region during May–June, which is relatively early in the dusty season. It can be noted that Plate 1 also shows noticeable aerosols over the north tropical Pacific Ocean (just north of the equator) in spring and early summer on the TOMS data, but missing in the POLDER AOT. Interestingly, similar to TOMS data, noticeable aerosols have also been observed by AVHRR in March, April, and May in the same region [Husar *et al.*, 1997]. Since this is a region with less influence from the aerosols originated over land, it is not clear whether this plume is related to a “real” aerosol signal or to other features (as a signal related to the information retrieved by each instrument, for example).

#### 4. Comparison for Selected Sites

Based on the monthly images presented on Plate 1, we select eight oceanic sites under the influence of different aerosol continental sources and for which it is interesting to investigate the consistency of the TOMS and POLDER retrieval. The positions of these sites are indicated on the TOMS images shown in Plate 1 (white triangles). Three sites are located in the Atlantic Ocean (NW Africa, Gulf of Guinea, and Angola), one site is located in the Mediterranean Sea (eastern Mediterranean), two sites in the Indian Ocean (Arabian Sea and Bay of Bengal), and two sites in the Pacific Ocean (East China Sea and Sea of Japan). For this comparison the positive values of the TOMS AI, the POLDER AOT, and Angström coefficients are averaged over a box of  $2^\circ$  in latitude and  $2.5^\circ$  in longitude. The latitude and longitude of the center of each box is given in Table 1. In Table 1 the sites are classified by order of increasing averaged Angström coefficients. Thus the lowest Angström retrieved by POLDER are over NW Africa, Arabian Sea, Gulf of Guinea, and eastern Mediterranean; this is consistent with the location of these regions, relatively close to desert areas. By contrast, the highest POLDER Angström coefficients are retrieved over the Pacific Ocean (Sea of Japan and East China Sea), Bay of Bengal, and Angola. In these regions the aerosol content appears to be dominated by smaller particles, similar to those emitted by biomass burning fires (as in the Angola region).

##### 4.1. Monthly Variations

Figure 1 shows the monthly mean values of the TOMS-derived AI and POLDER AOT at 670 nm for the eight locations described above. Since the TOMS Earth Probe continued to provide data after the POLDER ADEOS failure in late June 1997, the AI is reported until October 1997. Figure 1 shows, in general, a good correspondence between the POLDER and TOMS temporal variability. Table 1 shows that the NW Africa and the Gulf of Guinea are the regions where the averaged TOMS AI and POLDER AOT are the highest over the period November 1996 to June 1997.

For the NW Africa box, Figure 1 shows that POLDER and TOMS present maximums in February and June, in agreement with the Saharan dust transport over this region that occurs both in winter and summer at higher altitude [Chiapello *et al.*, 1995; Prospero and Carlson, 1972]. In the region of Gulf of Guinea, the largest aerosol amounts are recorded from January to March, in agreement with previous observations from AVHRR in this region [Husar *et al.*, 1997]. This maximum can be related to winter transport of dust over the Gulf of Guinea, but biomass-burning products are likely to contribute to the aerosol content as well. For the SW Africa region off the coast of Angola, TOMS shows a maximum AI occurring in austral winter (June–September), the dry season in southern Africa. This maximum does not appear as intense in the variations of the POLDER AOT at least for June. However, the mean Angström coefficient derived from POLDER over this region during May–June clearly shows the influence of small particles (see Table 1), as expected under the influence of biomass burning aerosols. The monthly averaged AOT derived from AVHRR in this region shows maximum values in austral winter (August–September) [Husar *et al.*, 1997], in agreement with the seasonal variations of the TOMS AI. In eastern Mediterranean and Arabian Sea, two sites impacted by desert dust, the aerosol contents retrieved by both TOMS and POLDER appear more limited in intensity. Over the Mediterranean region the maximum of POLDER AOT and TOMS AI appear from April to June. This seasonality is in agreement with the dust transport from North Africa which is known to be the greatest during spring and summer [Bergametti *et al.*, 1989a, 1989b; Moulin *et al.*, 1998]. For the Arabian Sea region, the occurrence of maximum in June (from POLDER AOT) and July–August (from TOMS AI) is very consistent with previous observations from AVHRR [Husar *et al.*, 1997]. In the Pacific region (i.e., for the sites East China Sea and Sea of Japan) the seasonal variations of the POLDER AOT and the TOMS AI show maximum during the spring months. Asia is known to be an important source of desert dust, anthropogenic sulfur, and biomass burning products. Aerosol measurements in the North Pacific Ocean have shown that the concentrations of these constituents generally present maximum in spring [Prospero *et al.*, 1989; Savoie *et al.*, 1989; Arimoto *et al.*, 1996; Carmichael *et al.*, 1997], in agreement with the observations of TOMS and POLDER. In the Bay of Bengal both TOMS and POLDER record a peak in March. Considering the rather high values of the POLDER Angström associated to this peak (about 0.8, see Table 1), we can suspect it to be related to biomass burning activities in Bangladesh and northern Burma, which seem to occur during March through May [Hao and Liu, 1994].

##### 4.2. Relations Between the TOMS AI and POLDER AOT

For each of the sites discussed above, Table 2 reports the correlation coefficients and slopes of the relationship obtained between the TOMS AI and the POLDER AOT computed at 440, 670, and 865 nm, along with the number of days available with coincident POLDER and TOMS data for each site. The POLDER AOT at 440 nm is computed from the AOT at 865 nm and the Angström coefficient, which is assumed to be unchanged over the ranges 670–865 and 440–865 nm. The results are reported both over an 8-month time period and over a 2-month timescale. Our results indicate that, depending on the season, the correlation obtained between the TOMS AI and

**Table 1.** POLDER Mean Angström Coefficients (670–865 nm), POLDER Mean Aerosol Optical Thickness at 670 nm, and TOMS Mean Aerosol Index for Each Oceanic Region

Time Period	POLDER Mean Angström	POLDER Mean AOT 670 nm	TOMS Mean AI
<i>NW Africa, 16°N, 22.5°W</i>			
Global	0.22	0.40	0.78
Nov.–Dec.	0.22	0.28	0.70
Jan.–Feb.	0.20	0.53	0.90
March–April	0.26	0.44	0.58
May–June	0.22	0.50	0.98
<i>Arabian Sea, 18°N, 58.75°E</i>			
Global	0.37	0.27	0.30
Nov.–Dec.	0.31	0.18	0.16
Jan.–Feb.	0.28	0.25	0.25
March–April	0.51	0.28	0.30
May–June	0.31	0.33	0.46
<i>Gulf of Guinea, 5°N, 20°W</i>			
Global	0.40	0.42	0.83
Nov.–Dec.	0.49	0.26	0.74
Jan.–Feb.	0.36	0.62	1.15
March–April	0.41	0.42	0.76
May–June	-	-	-
<i>Eastern Mediterranean, 35°N, 25°E</i>			
Global	0.53	0.19	0.31
Nov.–Dec.	0.48	0.18	0.36
Jan.–Feb.	0.35	0.14	0.24
March–April	0.62	0.19	0.21
May–June	0.65	0.23	0.36
<i>East China Sea, 21°N, 118.75°E</i>			
Global	0.55	0.22	0.29
Nov.–Dec.	-	-	-
Jan.–Feb.	-	-	-
March–April	0.58	0.28	0.50
May–June	0.46	0.17	0.15
<i>Angola, 10°S, 10°E</i>			
Global	0.68	0.25	0.57
Nov.–Dec.	-	-	-
Jan.–Feb.	0.25	0.25	0.77
March–April	-	-	-
May–June	0.83	0.26	0.53
<i>Bay of Bengal, 19°N, 87.5°E</i>			
Global	0.73	0.35	0.43
Nov.–Dec.	0.71	0.29	0.33
Jan.–Feb.	0.76	0.32	0.28
March–April	0.81	0.40	0.76
May–June	0.48	0.45	0.36
<i>Sea of Japan, 40°N, 132.5°E</i>			
Global	0.78	0.25	0.53
Nov.–Dec.	0.53	0.17	0.49
Jan.–Feb.	0.56	0.19	0.54
March–April	1.03	0.31	0.54
May–June	1.09	0.38	0.60

The results are reported for the whole time period (November 1, 1996, to June 29, 1997, designated as "global") and for 2-month time periods. The lines with no data correspond to the lack of coincident days for POLDER and TOMS observations during the period. The latitude and longitude of the center of the box in which the comparison is performed are indicated in the first line. Each box has a size of 2° in latitude and 2.5° in longitude.

the POLDER AOT vary significantly. Figure 2 reports for each site the data from the season giving the best correlation between the TOMS AI and the POLDER AOT at 670 nm. In general, a good correlation is obtained during the period of maximum aerosol content detected by TOMS and POLDER. Thus in the NW Africa region the correlation coefficients are high in January–February and May–June ( $r$  above 0.84 at the three wavelengths), which are months associated with the maximum of TOMS AI and POLDER AOT (see Table 1). For the Arabian Sea and eastern Mediterranean regions the best correlation coefficients are obtained in May–June, which

is the period of aerosol peaks associated with maximum dust transport. It is striking to note that in the regions of Gulf of Guinea, East China Sea, and Angola, the correlation coefficients obtained when fitting the TOMS and POLDER data from the whole period are above 0.75 at 670 nm. However, Figure 2 shows that these correlations improve when plotting the data only for the period of the maximum concentrations. For the Bay of Bengal region a good correlation is obtained between TOMS and POLDER for the March–April time period, corresponding to the aerosol peaks. The Sea of Japan is

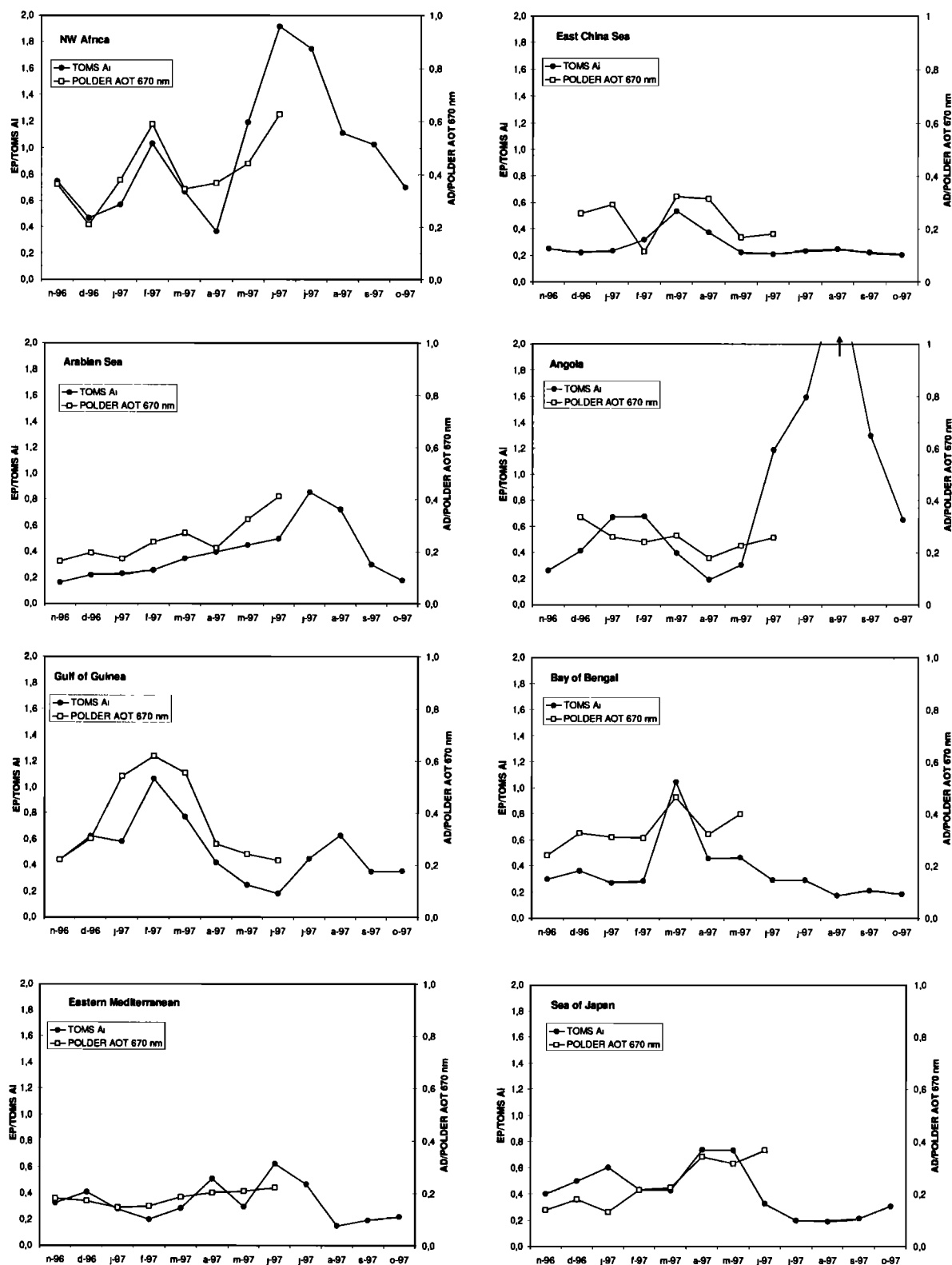


**Figure 1.** Monthly mean of Earth-Probe TOMS absorbing aerosol index and ADEOS POLDER aerosol optical thickness at 670 nm for various oceanic regions. The locations of the regions are reported in Table 1. Note that the aerosol optical thickness at 670 nm is computed from the POLDER aerosol optical thickness at 865 nm and the POLDER Angström coefficient (865–670 nm).

**Table 2.** Correlation Coefficients and Slopes of the Relationship Obtained Between the TOMS AI and the POLDER AOT at 865, 670, and 440 nm for Each Oceanic Region

Time Period	Number of Coincident Days	865 nm		670 nm		440 nm	
		Slope	<i>r</i>	Slope	<i>r</i>	Slope	<i>r</i>
NW Africa							
Global	42	1.7	0.67	1.6	0.67	1.5	0.68
Nov.-Dec.	20	1.4	0.48	1.4	0.52	1.3	0.57
Jan.-Feb.	9	2.8	0.86	2.7	0.85	2.4	0.84
March-April	5	0.9	0.66	0.9	0.71	0.8	0.76
May-June	8	2.7	0.86	2.7	0.87	2.7	0.88
Arabian Sea							
Global	62	1.2	0.65	1.1	0.64	0.8	0.59
Nov.-Dec.	13	-0.1	0.05	-0.1	0.09	-0.2	0.15
Jan.-Feb.	14	0.9	0.56	0.8	0.54	0.7	0.49
March-April	19	0.4	0.24	0.3	0.23	0.2	0.19
May-June	16	1.2	0.69	1.2	0.70	1.1	0.69
Gulf of Guinea							
Global	27	1.9	0.74	1.8	0.77	1.6	0.81
Nov.-Dec.	7	6.6	0.91	4.8	0.90	2.7	0.87
Jan.-Feb.	10	2.2	0.86	2.1	0.88	1.9	0.91
March-April	6	1.4	0.48	1.3	0.50	1.2	0.54
May-June	4	-	-	-	-	-	-
Eastern Mediterranean							
Global	67	2.6	0.74	2.2	0.70	1.4	0.56
Nov.-Dec.	18	1.1	0.58	1.1	0.56	0.8	0.47
Jan.-Feb.	16	-0.2	0.05	0.4	0.13	0.6	0.31
March-April	10	2.1	0.81	1.5	0.69	0.6	0.42
May-June	23	4	0.90	3.6	0.86	2.6	0.72
East China Sea							
Global	20	2	0.71	1.8	0.75	1.4	0.79
Nov.-Dec.	2	-	-	-	-	-	-
Jan.-Feb.	1	-	-	-	-	-	-
March-April	8	3	0.97	2.4	0.97	1.6	0.94
May-June	9	0.1	0.08	0.1	0.11	0.1	0.16
Angola							
Global	20	6.4	0.85	5	0.88	2.6	0.84
Nov.-Dec.	3	-	-	-	-	-	-
Jan.-Feb.	6	4.8	0.88	4	0.84	2.4	0.72
March-April	0	-	-	-	-	-	-
May-June	11	6.8	0.85	5	0.91	2.9	0.96
Bay of Bengal							
Global	78	1.6	0.50	1.4	0.55	1	0.57
Nov.-Dec.	22	0.1	0.06	0.1	0.07	0.1	0.08
Jan.-Feb.	27	0.5	0.27	0.4	0.28	0.2	0.29
March-April	21	3.6	0.78	3	0.86	1.8	0.87
May-June	8	1.4	0.71	1.3	0.68	1	0.61
Sea of Japan							
Global	66	1.4	0.37	1	0.40	0.6	0.42
Nov.-Dec.	19	2.3	0.55	2.1	0.58	1.8	0.61
Jan.-Feb.	16	1.8	0.32	1.2	0.27	0.6	0.18
March-April	22	1.4	0.30	1.4	0.43	1	0.58
May-June	9	1.8	0.50	1.2	0.47	0.6	0.42

The number of days available with coincident TOMS and POLDER data is indicated. The results are reported for the whole time period (November 1, 1996, to June 29, 1997) and for 2-month time periods.

the only site for which all the correlation coefficients between POLDER and TOMS are below 0.6. Figure 2 shows that at this site the POLDER retrieved AOT is below 0.35, a rather moderate value. As a possible explanation to the absence of correlation between TOMS and POLDER at this site, several studies of aerosol in the Pacific Ocean have indicated that this region is impacted by aerosols from different sources, especially mineral dust and sulfates from industrial activities, which are likely to be internally mixed [Horai *et al.*, 1993; Parungo *et al.*, 1995; Dentener *et al.*, 1996]. Such a mixture will complicate the use of AI from TOMS in this region.

Figure 2 and Table 2 show that depending on the location and the wavelength we obtain different slopes for the relationship between the TOMS AI and POLDER AOT. At 440 nm the slopes of the best fit obtained for the NW Africa, Gulf of Guinea, and eastern Mediterranean sites range between 1.9 and 2.7 (see Table 2). These values are in the same range as those obtained by Hsu *et al.* [1999] when comparing the TOMS AI to sunphotometer measurements of AOT performed in the Sahel and NW Atlantic regions. For the Arabian Sea region the slope of the fit obtained in May-June is significantly lower (1.1 at 440 nm). For the regions characterized by higher



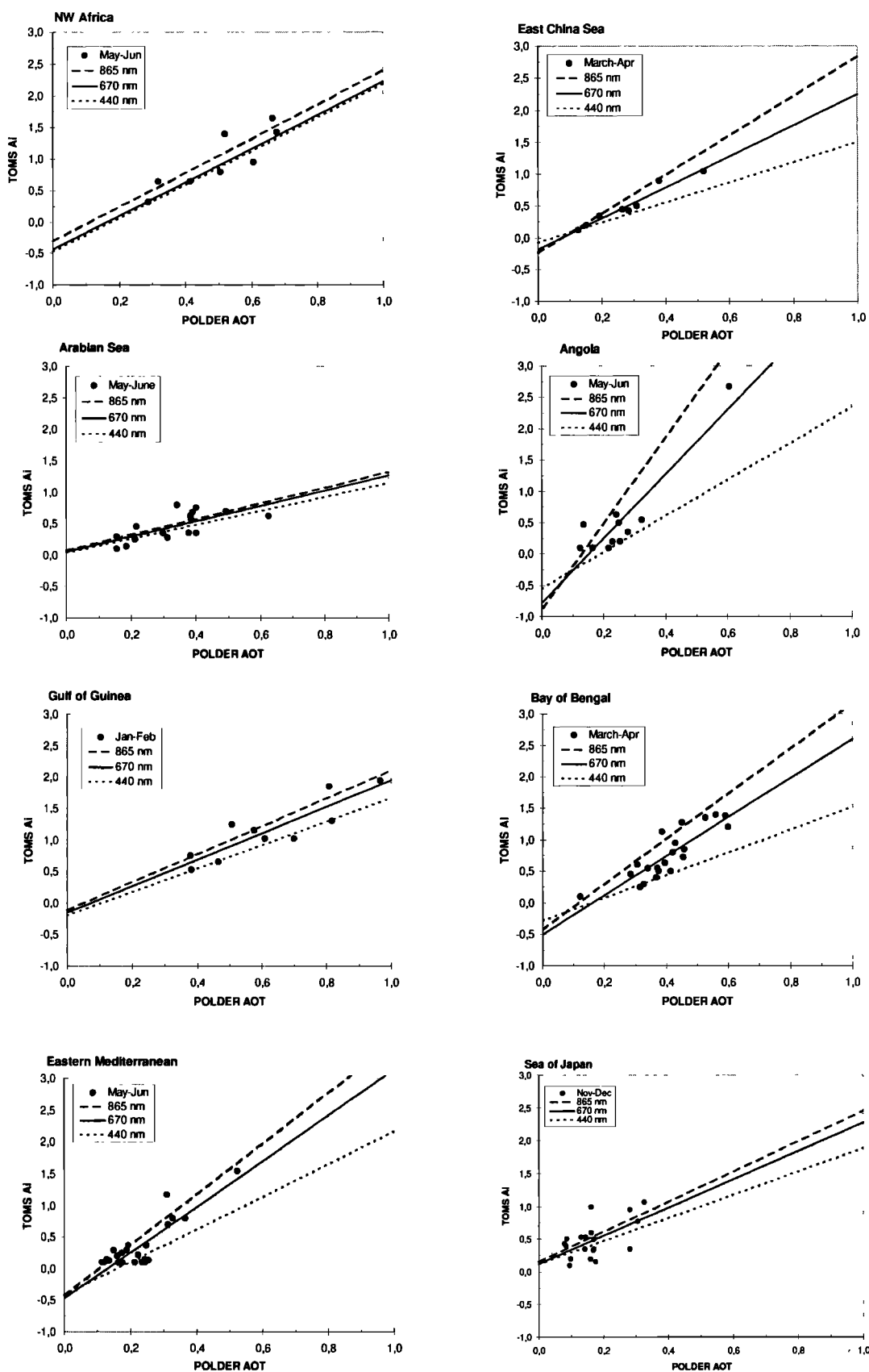


**Figure 2.** Comparison of Earth-Probe TOMS absorbing aerosol index with ADEOS POLDER aerosol optical thickness at 670 nm for the different oceanic regions described in Table 1 and for the time period which allows the best linear relation (see Table 2). The solid lines represent the regression fits to the data (POLDER AOT at 670 nm). The dotted and dashed lines represent the fits obtained with POLDER AOT at 440 and 865 nm, respectively. The equations and correlation coefficients for the regression lines are reported in Table 2.

Angström coefficients, that is, East China Sea, Angola, and Bay of Bengal, the slopes of the best fit range from 1.6 to 2.9 at 440 nm. The value of 2.9 obtained for the Angola region in May–June is relatively high compared to the one retrieved by Hsu *et al.* [1999] using AOT measured in Zambia during the burning season (June–October). However, the differences in the season and range of AOT (ours are below 0.6) may be sufficient to explain these deviations in the relation between the TOMS AI and the AOT.

Our comparisons suggest that, depending on the geographical situation, a given amount of aerosol optical thickness can lead to a large range of AI (overall the slopes range between 1.1 and 2.9 at 440 nm). The two parameters which are known to play dominant roles in the relationship between the TOMS AI and AOT are the altitude of the aerosol layer and the single-scattering albedo (which depends on the nature of the aerosol) [Torres *et al.*, 1998; Hsu *et al.*, 1999]. These two parameters are likely to be variable from one region to another, which is probably sufficient to explain the variability of the TOMS AI – POLDER AOT relationship.

## 5. Conclusions

In this paper we investigate the relationship between the TOMS AI and the POLDER derived-AOT over oceans and in particular at eight sites located in the Atlantic Ocean, Mediterranean Sea, Indian Ocean, and Pacific Ocean. In general, the spatial distributions and monthly variations of the aerosol content derived from TOMS and POLDER are very consistent and also in good agreement with other instrument's observations over oceanic regions such as those from AVHRR [Husar *et al.*, 1997]. At all sites, with the exception of the Sea of Japan, our results indicate that, during the time period of maximum aerosol content, a linear correlation exists between the TOMS AI and POLDER AOT. In the region of the Sea of Japan we suspect the occurrence of mixtures of different aerosol types (i.e., mineral dust, soot, and sulfate) as an explanation of the poor correlation observed between TOMS and POLDER. Moreover, it can be noted that among all the sites, the POLDER AOT at the Sea of Japan has the lowest maximum value, and the highest averaged Angström coefficient.

Our results, although limited to an 8-month time period, suggest that TOMS and POLDER aerosol retrievals are very consistent over the oceanic regions under the influence of biomass burning aerosols and desert dust. The good correlation obtained between the POLDER AOT and the TOMS AI are remarkable considering the totally different approaches of the two instruments and the uncertainties inherent to each method. The results of these comparisons confirm that mineral dust and biomass-burning aerosol distributions can be retrieved using different techniques, either in the UV or in the visible range. The main advantage of the TOMS detection in the UV is to offer the retrieval of aerosol distributions over both continents and oceans. The principal limitation of this method is that the aerosol optical thickness of UV-absorbing aerosols cannot be derived without an assumption of the altitude of the aerosol layer. In contrast, POLDER allows the retrieval of physical quantities, that is, aerosol optical thickness and Angström coefficients, but at this point only over oceans. It certainly remains one of the main challenges in the field of aerosol remote sensing from space to retrieve optical thickness of aerosols over both continental and oceanic surfaces.

**Acknowledgments.** The authors would like to thank the CNRS and the CNES for their financial support. We also thank Olivier Boucher and two anonymous referees for their useful comments.

## References

- Andreae, M. et al., Biomass burning in the global environment: First results from the IGAC-BIBEX field campaign STARE/TRACE A/SAFARI 92, in *Global Atmospheric-Biospheric Chemistry*, edited by R.G. Prinn, pp. 83–101, Plenum, New York, 1994.
- Arimoto, R., R.A. Duce, D.L. Savoie, J.M. Prospero, R. Talbot, J.D. Cullen, U. Tomza, N.F. Lewis, and B.J. Ray, Relationships among aerosol constituents from Asia and the North Pacific during PEM-West A, *J. Geophys. Res.*, **101**, 2011–2024, 1996.
- Bergametti, G., A.-L. Dutot, P. Buat-Menard, R. Losno, and E. Remoudaki, Seasonal variability of the elemental composition of atmospheric aerosol particles over the northwestern Mediterranean, *Tellus, Ser. B.*, **41**, 353–361, 1989a.
- Bergametti, G., L. Gomes, E. Remoudaki, M. Desbois, D. Martin, and P. Buat-Menard, Present transport and deposition patterns of African dusts to the North Western Mediterranean, in *Paleoclimatology and Paleometeorology: Modern and Past Patterns of Global Atmospheric Transport*, pp. 227–252, Kluwer Acad., Norwell, Mass., 1989b.
- Carmichael, G.R., M.S. Hong, H. Ueda, L.L. Chen, K. Murano, J.K. Park, H. Lee, Y. Kim, and S. Shim, Aerosol composition at Cheju Island, Korea, *J. Geophys. Res.*, **102**, 6047–6061, 1997.
- Chiapello, I., G. Bergametti, L. Gomes, B. Chatenet, F. Dulac, J. Pimenta, and E. Santos Soares, An additional low layer transport of Sahelian and Saharan dust over the northeastern Tropical Atlantic, *Geophys. Res. Lett.*, **22**, 3191–3194, 1995.
- Chiapello, I., J.M. Prospero, J.R. Herman, and N.C. Hsu, Detection of mineral dust over the North Atlantic Ocean and Africa with Nimbus-7/TOMS, *J. Geophys. Res.*, **104**, 9277–9291, 1999.
- Dentener, F.J., G.R. Carmichael, Y. Zhang, J. Lelieveld, and P.J. Crutzen, Role of mineral aerosol as a reactive surface in the global troposphere, *J. Geophys. Res.*, **101**, 22,869–22,889, 1996.
- Deuzé, J.L., M. Herman, P. Goloub, D. Tanré, and A. Marchand, Characterization of aerosols over ocean from POLDER/ADEOS-1, *Geophys. Res. Lett.*, **26**, 1421–1424, 1999.
- Goloub, P., D. Tanré, J.L. Deuzé, M. Herman, A. Marchand, and F.M. Bréon, Validation of the first algorithm applied for deriving the aerosol properties over the ocean using the POLDER/ADEOS measurements, *IEEE Trans. Geosci. Remote Sens.*, **37**, 1586–1596, 1999.
- Hao, W.M., and M.H. Liu, Spatial and temporal distribution of tropical biomass burning, *Global Biogeochem. Cycles*, **8**, 495–503, 1994.
- Herman, J.R., and E. Celarier, Earth's surface reflectivity climatology at 340–380 nm from TOMS data, *J. Geophys. Res.*, **102**, 28,003–28,012, 1997.
- Herman, J.R., P.K. Bhartia, O. Torres, C. Hsu, C. Seftor, and E. Celarier, Global distribution of UV-absorbing aerosols from Nimbus 7/TOMS data, *J. Geophys. Res.*, **102**, 16,911–16,922, 1997.
- Holben, B.N., et al., AERONET-A federated instrument network and data archive for aerosol characterization, *Remote Sens. Environ.*, **66**, 1–16, 1998.
- Horai, S., I. Minari, and Y. Migita, Aerosols composition in Kagoshima, in *Annual Report of the Kagoshima Prefectural Institute*, vol. 9, 1993.
- Hsu, N.C., J.R. Herman, O. Torres, B.N. Holben, D. Tanré, T.F. Eck, A. Smirnov, B. Chatenet, and F. Lavenu, Comparisons of the TOMS aerosol index with Sun-photometer aerosol optical thickness: Results and applications, *J. Geophys. Res.*, **104**, 6269–6279, 1999.
- Husar, R.B., J.M. Prospero, and L.L. Stowe, Characterization of tropospheric aerosols over the oceans with the NOAA advanced very high resolution radiometer optical thickness operational product, *J. Geophys. Res.*, **102**, 16,889–16,909, 1997.
- Jankowiak, I., and D. Tanré, Satellite climatology of Saharan dust outbreaks, *J. Clim.*, **5**, 646–656, 1992.
- Kaufman, Y.J., D. Tanré, H.R. Gordon, T. Nakajima, J. Lenoble, R. Frouin, H. Grassl, B.M. Herman, M.D. King, and P.M. Teillet, Passive remote sensing of tropospheric aerosol and atmospheric correction for the aerosol effect, *J. Geophys. Res.*, **102**, 16,815–16,830, 1997.

- Morales, C. (Ed.), *Saharan Dust: Mobilization, Transport, Deposition*, John Wiley, New York, 1979.
- Moulin, C., F. Guillard, F. Dulac, and C.E. Lambert, Long-term daily monitoring of Saharan dust load over ocean using Meteosat ISCCP-B2 data, 1, Methodology and preliminary results for 1983-1994 in the Mediterranean, *J. Geophys. Res.*, **102**, 16,947-16,958, 1997a.
- Moulin, C., F. Dulac, C.E. Lambert, P. Chazette, I. Jankowiak, B. Chatenet, and F. Lavenu, Long-term daily monitoring of Saharan dust load over ocean using Meteosat ISCCP-B2 data, 2, Accuracy of the method and validation using Sun photometer measurements, *J. Geophys. Res.*, **102**, 16,959-16,969, 1997b.
- Moulin, C., et al., Satellite climatology of African dust transport in the Mediterranean atmosphere, *J. Geophys. Res.*, **103**, 13,137-13,144, 1998.
- Parungo, F., Y. Kim, C.J. Zhu, J. Harris, R. Schnell, X.S. Li, D.Z. Yang, M.Y. Zhou, Z. Chen, and K. Park, Asian dust storms and their effects on radiation and climate, *STC Rep. 2906*, Natl. Oceanic and Atmos. Admin. Air Resour. Lab., Silver Spring, Md., 1995.
- Prospero, J.M., and T.N. Carlson, Vertical and areal distribution of Saharan dust over the western equatorial North Atlantic Ocean, *J. Geophys. Res.*, **77**, 5255-5265, 1972.
- Prospero, J.M., R.A. Glaccum, and R.T. Nees, Atmospheric transport of soil dust from Africa to South America, *Nature*, **289**, 570-572, 1981.
- Prospero, J.M., M. Uematsu, and D.L. Savoie, Mineral aerosol transport to the Pacific Ocean, in *Chemical Oceanography*, vol. 10, edited by J.P. Riley, R. Chester, and R.A. Duce, pp. 188-218, Academic, San Diego, Calif., 1989.
- Savoie D.L., J.M. Prospero, and E.S. Saltzman, Nitrate, non-seasalt sulfate and methanesulfonate over the Pacific Ocean, in *Chemical Oceanography*, vol. 10, edited by J.P. Riley, R. Chester, and R.A. Duce, pp. 219-250, Academic, San Diego, Calif., 1989.
- Swap, R., S. Ulanski, M. Cobbett, and M. Garstang, Temporal and spatial characteristics of Saharan dust outbreaks, *J. Geophys. Res.*, **101**, 4205-4220, 1996.
- Torres, O., P.K. Bhartia, J.R. Herman, Z. Ahmad, and J. Gleason, Derivation of aerosol properties from satellite measurements of backscattered ultraviolet radiation: Theoretical basis, *J. Geophys. Res.*, **103**, 17,099-17,110, 1998.
- I. Chiapello, P. Goloub, A. Marchand, and D. Tanré, Laboratoire d'Optique Atmosphérique, Université des Sciences et Technologies de Lille, Bat. P5, 59655 Villeneuve d'Ascq Cedex, France. (chiapello@loa.univ-lille1.fr; goloub@loa.univ-lille1.fr; marchand@loa.univ-lille1.fr; tanre@loa.univ-lille1.fr)
- J. Herman and O. Torres, Laboratory for Atmospheres, NASA Goddard Space Flight Center, Code 916, Greenbelt, MD 20771 (herman@tparty.gsfc.nasa.gov; torres@tparty.gsfc.nasa.gov)

(Received May 14, 1999; revised September 20, 1999; accepted September 28, 1999.)